Nanoscale

RSC Publishing

PAPER

View Article Online
View Journal | View Issue

Published on 12 March 2013. Downloaded by Zhejiang University on 26/02/2014 07:47:31.

Cite this: *Nanoscale*, 2013, **5**, 4370

Bioinspired design and macroscopic assembly of poly(vinyl alcohol)-coated graphene into kilometers-long fibers†

Liang Kou and Chao Gao*

Nacre is characterized by its excellent mechanical performance due to the well-recognized "brick and mortar" structure. Many efforts have been applied to make nacre-mimicking materials, but it is still a big challenge to realize their continuous production. Here, we prepared sandwich-like building blocks of poly(vinyl alcohol) (PVA)-coated graphene, and achieved high-nanofiller-content kilometers-long fibers by continuous wet-spinning assembly technology. The fibers have a strict "brick and mortar" layered structure, with graphene sheet as rigid brick and PVA as soft mortar. The mortar thickness can be precisely tuned from 2.01 to 3.31 nm by the weight feed ratio of PVA to graphene, as demonstrated by both atomic force microscopy and X-ray diffraction measurements. The mechanical strength of the nacre-mimicking fibers increases with increasing the content of PVA, and it rises gradually from 81 MPa for the fiber with 53.1 wt% PVA to 161 MPa for the fiber with 65.8 wt% PVA. The mechanical performance of our fibers was independent of the molecular weight (MW) of PVA in the wide range of 2–100 kDa, indicating that low MW polymers can also be used to make strong nanocomposites. The tensile stress of fibers immersed in PVA 5 wt% solution reached *ca*. 200 MPa, surpassing the values of nacre and most of other nacre-mimicking materials. The nacre-mimicking fibers are highly electrically conductive (~350 S m^{-1}) after immersing in hydroiodic acid, enabling them to connect a circuit to illuminate an LED lamp.

Received 28th January 2013
Accepted 7th March 2013

DOI: 10.1039/c3nr00455d

www.rsc.org/nanoscale

Introduction

Organic–inorganic nanocomposites, combining the flexibility of organic polymers with the hardness and high strength of inorganic matter, are one of the most promising materials with wide applications. However, when the loading of inorganic nanofillers exceeds a certain fraction (generally lower than 10 wt %), the mechanical performance of composites would decline dramatically because of the formation of void defects and phase separation between polymers and nanofillers.[1] So it is extremely difficult to access high-performance nanocomposites with high content of nanofillers. Nevertheless, nacre solved this problem ideally by the formation of a "brick-and-mortar" (B&M) structure with 95–99 wt% inorganic platelet minerals (typically calcium carbonate, calcium phosphate and amorphous silica) and 1–5 wt% organic biopolymers (typically keratin, collagen and chitin) in the process of natural evolution.[2] Consequently, a number of works have been done to fabricate nacre-mimicking materials by employing inorganic montmorillonite,[3–6] ceramics,[7,8] layered double hydroxides (LDHs),[9] and biominerals[10] as bricks and organic polymers such as polyvinyl alcohol (PVA),[3] polyacrylamide (PAA),[4] polyimide (PI),[5] chitosan,[6,7] polymethyl methacrylate (PMMA),[8] and poly(styrene-4-sulfonate) (PSS)[9] as mortar. To make nacre-mimicking films, several protocols have been presented, including layer-by-layer deposition,[3] interface-assisted self-assembly,[7] vacuum filtration assisted self-assembly,[11] Langmuir–Blodgett self-assembly,[12] and freeze-drying assembly.[13]

Recently, graphene or graphene oxide (GO)-based nacre mimics have received particular interest due to the exceptional attributes of graphene such as ultrahigh fracture strength (~125 GPa) and Young's modulus (~1100 GPa) as well as good electrical conductivity.[14–20] Similar to the cases of other nanofillers, when the content of chemically reduced graphene (CRG) or GO was higher than 3 wt%, the composite generally became very brittle and its mechanical strength fell down.[17] Although Brinson and Liao's groups fabricated high-nanofiller-content GO@PVA film with highly ordered GO arrangement by vacuum filtration assisted assembly and casting techniques, the methods used were relatively time-consuming and confined to a small area of production.[11,21] In order to resolve the problem of

MOE Key Laboratory of Macromolecular Synthesis and Functionalization, Department of Polymer Science and Engineering, Zhejiang University, Hangzhou, 310027, China. E-mail: chaogao@zju.edu.cn

† Electronic supplementary information (ESI) available: More AFM and SEM images and electrical conductivities of CRG@PVA with different feed ratios, FTIR spectra, Raman and XPS results of GO, CRG and CRG@PVA, SEM images of CRG@PVA fibers with different diameters, SEM images and conductivity of CRG@PVA fibers with different MW of PVA, the tensile curve of CRG@PVA paper, and videos of graphene knot and spring. See DOI: 10.1039/c3nr00455d

This journal is © The Royal Society of Chemistry 2013

Published on 12 March 2013. Downloaded by Zhejiang University on 26/02/2014 07:47:31.

continuous preparation of nacre mimics, our group made a novel exploration and reported the first example of nacre-mimicking fibers composed of hyperbranched polymer (HP) and thermally-reduced graphene (TRG) by a wet-spinning strategy.[22] Since commercially available linear polymers and CRG are much more popular, achieving their continuous nacre-mimicking fibers is a dream target and is more promising in practical applications. However, accessing high CRG content nacre-mimicking fibers is much more challenging because CRG is much more difficult to disperse than TRG in solvents, especially in water.

Here, we prepared PVA-coated CRG (CRG@PVA) in water. Direct wet-spinning the hydrogel of CRG@PVA building blocks gave rise to continuous fibers up to kilometers long with well-aligned B&M microstructures. The content of CRG in the fibers could be adjusted by the feed ratio of PVA to CRG (R) in a range of 34–48 wt%. The mechanical strength of our nacre-mimicking fibers reached 200 MPa, obviously superior to that of nacre (120–150 MPa). We discovered that the mechanical performance of such fibers is independent of the molecular weight (MW) of PVA because the long-range, coordinated molecular motion was confined in nanochannels between two graphene sheets.

Experimental procedure

Materials

Graphite powder (40 μm) was obtained from Qingdao Henglide Graphite Co., Ltd. Concentrated H_2SO_4 (98%), $KMnO_4$, acetone and hydrazine hydrate (85%) were purchased from Sinopharm Chemical Reagent Co., Ltd. and used as received. 99+% hydrolyzed PVA (89–98 kDa) and 98–99% hydrolyzed PVA (31–50 kDa) were purchased from Sigma-Aldrich. 98% hydrolyzed PVA (16 kDa) was purchased from J&K Scientific Ltd and 75% hydrolyzed PVA (2 kDa) was purchased from Acros Organics. HI was obtained from Aladdin Chemistry Co., Ltd.

Characterization

Thermogravimetric analysis (TGA) was carried out on a Perkin-Elmer Pyris 6 TGA instrument under nitrogen with a heating rate of 10 °C min^{-1}. Fourier transform infrared spectra (FTIR) were recorded on BRUKER VECTOR 22 spectrometer. Scanning electron microscopy (SEM) images were measured using a Hitachi S4800 field emission SEM system. Raman measurements were carried out using a LabRam-1B Raman spectroscope equipped with a 632.8 nm laser source. X-ray diffraction (XRD) was carried out on a X'Pert PRO diffractometer equipped with Cu Kα radiation (40 kV, 40 mA). Atomic force microscopy (AFM) measurements were performed using a Digital Instrument Nanoscope IIIa scanning probe microscope, operating in the tapping mode, with samples prepared by spin-coating sample solutions onto freshly cleaved mica substrates at 2500 rpm. Electrical conductivities were measured using a four-probe resistivity instrument (RTS-4, PROBES TECH) and two-probe resistivity-measuring instrument. Mechanical tests were carried out using Regar RWT10. X-ray photoelectron spectroscopy (XPS) measurements were performed with a RBD upgraded PHI-5000C ESCA system (Perkin-Elmer) with Mg Kα radiation (h = 1253.6 eV) at a power of 250 W. The glass-transition temperature (T_g) and melting temperature (T_m) of samples were investigated by differential scanning calorimetry (DSC) using a NETZSCH STA-409PC instrument. SAXS tests were carried out at Shanghai Synchrotron Radiation Facility (SSRF), by using a fixed wavelength of 0.124 nm, a sample to detector distance of 5 m, and an exposure time of 300 s.

Preparation of water-soluble CRG@PVA building blocks

GO was prepared according to the previously published protocol.[23,24] We prepared a series of CRG@PVA with R of PVA to GO ranging from 20 to 10, 5, 2.5, 2.125, 1.75 and 1/1. In a typical procedure for preparing CRG@PVA with M_w of 89–98 kDa (CRG@PVA 100K), 20 g PVA was added to a 1000 mL round-bottom flask containing 500 mL de-ionized water followed by heating at 80 °C until PVA was completely dissolved. After adding 125 mL GO aqueous dispersion (8 mg mL^{-1}) to the solution of PVA, it was stirred for 10 h. Then 1 mL hydrazine solution (85%) was added to the dispersion and stirred for 1 h at 95 °C. The neat CRG@PVA building blocks were obtained by repeated centrifugation (23 294g RCF) and hot water washing to completely remove the unattached free polymer. To control the coating density, R was altered from 20 to 10, 5, 2.5, 2.125, 1.75 and 1/1 to prepare CRG@PVA 20, CRG@PVA 10, CRG@PVA 5, CRG@PVA 2.5, CRG@PVA 2.125, CRG@PVA 1.75 and CRG@PVA 1. Unless specifically noted, CRG@PVA refers to CRG@PVA 20 with M_w of 89–98 kDa. Moreover, PVA with different M_w including 31–50 kDa, 16 kDa and 2 kDa were also employed to functionalize CRG to obtain CRG@PVA 50K, CRG@PVA 16K, and CRG@PVA 2K with R of 20/1.

Preparation of CRG@PVA papers by vacuum-assisted filtration assembly

A 10 mL CRG@PVA dispersion (1 mg mL^{-1}) was sonicated (40 kHz) for 0.5 h and filtered through a cellulose film (0.22 μm pore size). The as-prepared CRG@PVA paper supported on the cellulose film was placed in a vacuum oven at 80 °C for 12 h, and finally the cellulose film was dissolved in acetone to get the free-standing CRG@PVA paper.

Preparation of continuous CRG@PVA fibers by wet-spinning assembly

CRG@PVA dispersed in water (25–50 mg mL^{-1}) was loaded into a 5 mL plastic syringe with a spinning nozzle (PEEK tube with diameter of 60, 100, 160 μm), and injected into an acetone bath by an injection pump (20 mL min^{-1}). After coagulation for 15 minutes, the fibers were drawn out and collected on scroll and dried for 12 h at 80 °C under vacuum.

Results and discussion

To spin continuous, smooth and ultralong graphene-based composite fibers, excellent solubility of building blocks is of the essence.[22] Without the stabilization of PVA, CRG could not be dispersed in water at all (Fig. 1H), while CRG was dispersed in

Published on 12 March 2013. Downloaded by Zhejiang University on 26/02/2014 07:47:31.

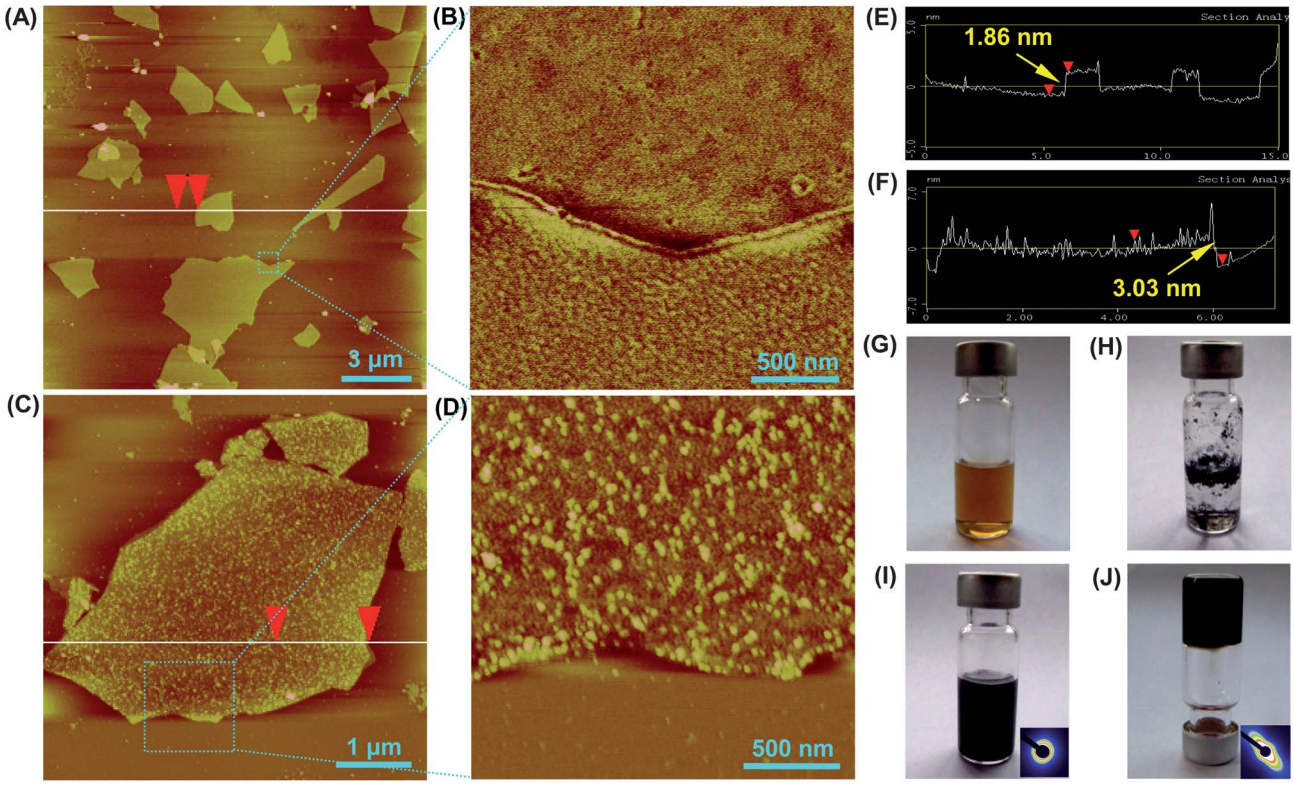

Fig. 1 AFM images of CRG@PVA with $R = 1.75$ (A and B) and 20 (C and D); E and F are the height profiles of A and C, respectively. Digital photographs of aqueous solutions of GO (G), CRG (H), CRG@PVA (I) and the spinning dope of CRG@PVA hydrogel (J); the insets of (I) and (J) are SAXS 2D patterns of CRG@PVA diluted aqueous solution and spinning dope, respectively.

water very well with sufficient PVA (Fig. 1I). We investigated the minimum amount of PVA needed to stabilize CRG in water. A low content of PVA ($R = 1/1$) directly led to precipitation of CRG in water after reducing GO by hydrazine. The precipitate could not be spun into fiber but could still form paper by vacuum filtration. When was R increased to a critical value of 1.75/1, the dispersion was stable and no obvious sediment was observed. AFM images of CRG@PVA 1.75 reveal that PVA chains are tiled on the surfaces of CRG and the height of build blocks is 1.86 nm (Fig. 1A, B and E), obviously higher than that of CRG and pristine GO (~0.8 nm).[25] The surface morphology and the height of the building blocks of CRG@PVA changed gradually with an increasing amount of PVA (Fig. S1†). For CRG@PVA with R of 20, PVA chains are attached on the surfaces of CRG as nanoclusters and the height increases to 3.03 nm (Fig. 1C, D and F). We investigated the interaction mechanism between PVA and CRG by XPS and FTIR. As shown in Fig. S2,† the oxygen content decreases from 27.2% for GO to 15.6% for the neat CRG. The carboxylic groups on CRG are still found after the hydrazine reduction in the FTIR spectrum of CRG@PVA (see Fig. S3†),[26] but the absorption peak is red shifted from 1731 to 1713 cm^{-1} because of the hydrogen bonding between CRG and PVA.[27] So PVA macromolecules are coated on CRG by hydrogen bonding interactions, making CRG well dispersible in water (>20 mg mL^{-1}). We found that CRG@PVA even formed a hydrogel when the concentration is higher than ~25 mg mL^{-1} (Fig. 1J).

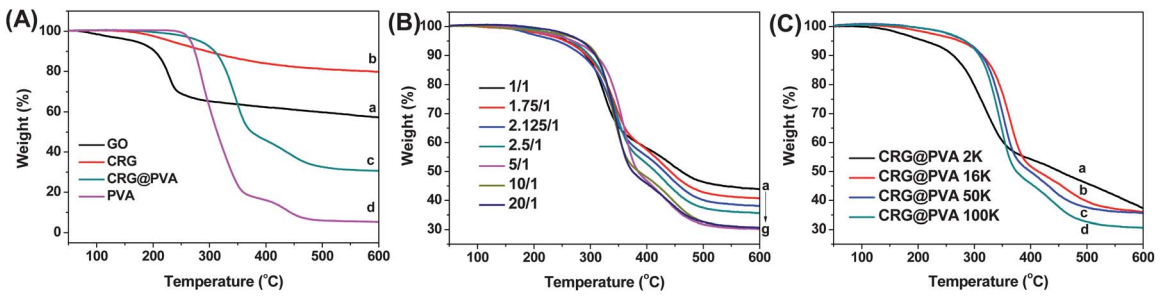

Fig. 2 (A) TGA curves of GO (a), CRG (b), CRG@PVA (c) and pure PVA (d). (B) TGA curves of CRG@PVA with different R (1/1–20/1 represented by a–g, respectively). (C) TGA curves of CRG@PVA with different M_w from 2K (a) to 16K (b), 50K (c) and 100K (d).

This journal is © The Royal Society of Chemistry 2013

Published on 12 March 2013. Downloaded by Zhejiang University on 26/02/2014 07:47:31.

Thermogravimetric analyses (TGA) were performed to weigh the amount of coated PVA (Fig. 2A). GO start to pyrolyse at 153 °C because of the decomposition of oxygen-containing groups, and 42.7% weight loss is observed at 600 °C. Compared with GO, CRG exhibits 20.2% weight loss at 600 °C without an obvious weight-loss step, indicating the efficient chemical reduction by hydrazine.[28] In addition, the thermal stability of PVA is highly enhanced (~17 °C) by coating on CRG and the 5% decomposition temperature increased from 266 °C for pure PVA to 283 °C for CRG@PVA. Such an improvement is mainly caused by the scavenger role of graphene for decomposed radicals[29] and the physical barrier effect of CRG which slows down the diffusion of pyrolysis products.[16] Generally, the percent fraction of coated PVA (f_{PVA}) increased with increasing R. For $R = 1/1$, almost all of the added PVA macromolecules were absorbed on the surfaces of CRG and the corresponding f_{PVA} was 49.0 wt%. At the critical R (1.75/1) for the spinning of CRG, the f_{PVA} is 53.1%, and it reached a saturated absorption as R rose to 5/1 (Fig. 2B). The f_{PVA}s for all samples with different R values are summarized in Table 1. The effect of the M_w of PVA on the saturated absorption was also investigated. Due to the M_w difference of the feeding PVA, the saturated absorption f_{PVA}s are 65.8%, 59.1%, 58.7%, and 56.9% for CRG@PVA 100K, CRG@PVA 50K, CRG@PVA 16K, and CRG@PVA 2K, respectively (Fig. 2C).

Utilizing the PVA-stabilized CRG as building blocks, we constructed nacre-mimicking papers with controlled thickness of mortar by simply adjusting R. Fig. 3A shows well-packed layers through the entire cross-section of the paper sample. The amplified image shows that the polymer is coated on the surface of CRG densely and uniformly (Fig. 3B and S4†), forming perfect B&M structures, as illustrated by cartoon in Fig. 3C. CRG@PVA with $R = 1$ could only form brittle paper due to its poor dispersibility in water, while CRG@PVA with higher Rs gave rise to flexible and robust papers because of their much better dispersibility. The layer-to-layer distance (d) of the nacre mimics was measured by XRD (Fig. 3D–I). As listed in Fig. 3F, the d increases gradually from 2.01 to 3.31 nm with increasing R from 1.75/1 to 20/1, very close to the thickness of individual building blocks measured by AFM (1.86–3.03 nm). Notably, every sample possesses a second order peak with d two times bigger than that of the first order peak (Fig. 3D),[30] suggesting uniformly and regularly packed B&M structures for the nacre-mimicking papers. It can be explained by Bragg's equation ($d = n\lambda/2\sin\theta$) and the two peaks are corresponding to $n = 1$ and 2, respectively. Besides R, PVA with distinct M_w influences d as well (Fig. 3G–I). For CRG@PVA 2K, d is 2.17 nm, while for CRG@PVA 16K, CRG@PVA 50K and CRG@PVA 100K, ds are 2.42, 2.51 and 3.31 nm, respectively.

Since poorly dispersed CRG and a very diluted dispersion could be used to fabricate graphene papers/films by filtration or drop casting methods, almost all of the published reports focused on films.[31,32] On the contrary, it is extremely difficult to access a continuous CRG fiber because high concentration is required in such a case.[33–35] Hence, no report has been published yet on fibers made from neat CRG and functionalized CRG. Based on the good dispersibility of our CRG@PVA, we tried to produce fibers by a wet-spinning assembly approach. Scheme 1 shows the process of (i) formation of CRG@PVA building blocks, (ii) pre-alignment of CRG@PVA in a highly concentrated liquid crystalline spinning dope, and (iii) continuous wet-spinning of CRG@PVA by injection into the coagulating bath. After coagulating for 15 min, the fiber was drawn out and scrolled on a winding drum.

The diameter of the fiber is even (Fig. 4A) and can be readily tuned from 30 to 100 μm (Fig. S6†) by changing the size of spinning nozzle. The surface displays wrinkles (Fig. 4B and C), which is quite similar to the case of neat graphene fibers.[36] The cross profile of the fiber shows the strict B&M structures built with alternative CRG and PVA layers (D–F), as schematically illustrated in Fig. 4I. The well-aligned layered structure is attributable to pre-alignment of the CRG@PVA dispersion, which is proved by small-angle X-ray scattering (SAXS) (Fig. 1J). As the concentration of the dispersion increased, the corresponding 2D patterns transformed from a blank diffusive signal (Fig. 1I) to an elliptical pattern with a larger axial ratio (with concentration higher than 4 mg mL^{-1}) (Fig. 1J), indicating the increasing degree of orientation in the CRG dispersion.

Table 1 Preparation conditions and selected results for CRG@PVA fibers

Fiber code	M_w (g mol^{-1})	R	f_{PVA} (wt%)	d (nm)	σ (MPa)	E (GPa)	Conductivity (S m^{-1})
CRG@PVA 1	100K	1.75	53.1	2.01	81	8.9	0.860
							350[a]
CRG@PVA 2	100K	2.125	56.5	2.06	88	8.0	0.790
CRG@PVA 3	100K	2.5	60.1	2.45	102	9.9	0.504
CRG@PVA 4	100K	5	65.6	2.89	122	10.4	0.107
CRG@PVA 5	100K	10	65.7	3.04	138	7.9	0.103
CRG@PVA 6	100K	20	65.8	3.31	161	9.9	0.013
					199[b]	17.1[b]	
					140[c]	5.4[c]	
CRG@PVA 7	50K	20	59.1	2.51	162	10.0	0.022
CRG@PVA 8	16K	20	58.7	2.42	158	10.8	0.036
CRG@PVA 9	2K	20	56.9	2.17	162	10.4	0.103

[a] The fiber reduced by hydroiodic acid. [b] The fiber was further immersed in 5 wt% PVA aqueous. [c] The resulting fiber was immersed in water.

Published on 12 March 2013. Downloaded by Zhejiang University on 26/02/2014 07:47:31.

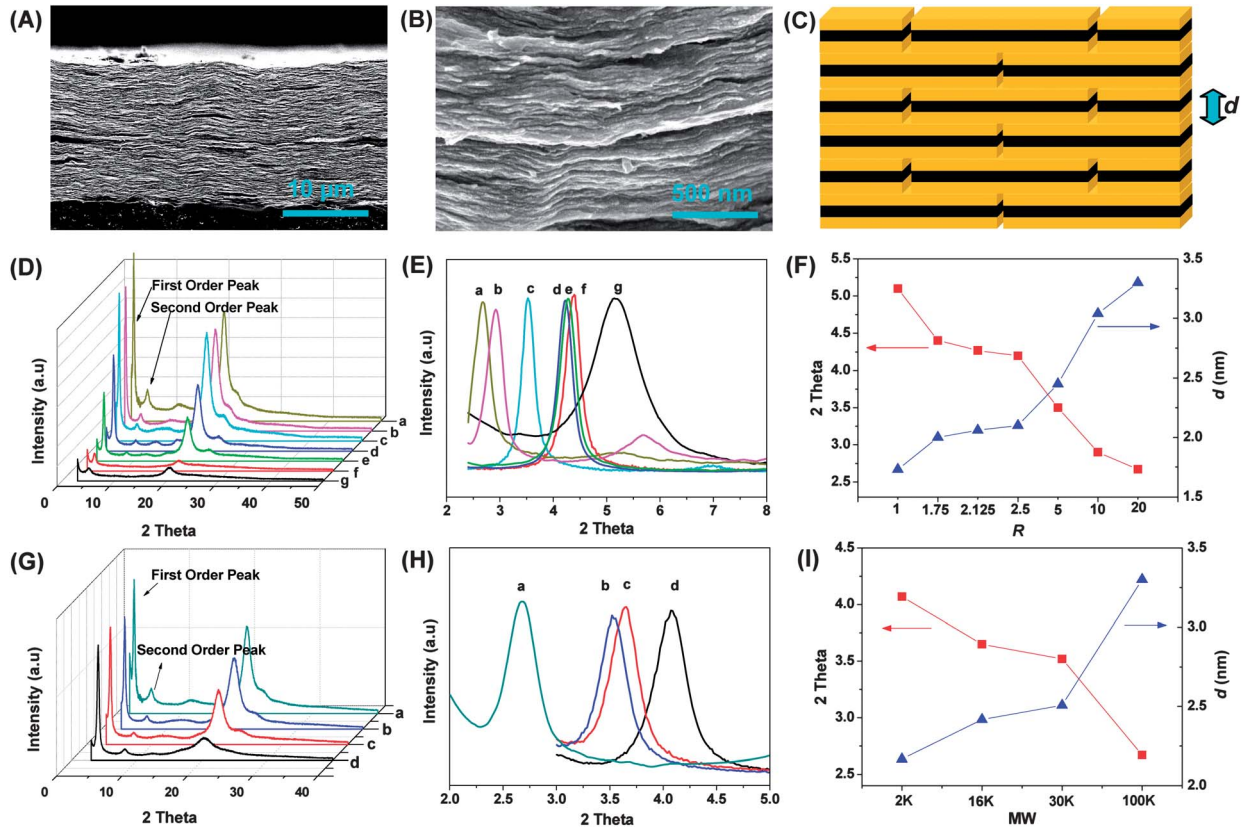

Fig. 3 (A) SEM image of the side view of CRG@PVA paper. (B) The magnified side view of (A). (C) Cartoon diagram of the B&M structure of CRG@PVA, the dark color represents CRG while the yellow denotes PVA. (D–F) XRD results of CRG@PVA with *R* from 1 to 1.75, 2.125, 2.5, 5, 10 and 20, represented by a–g respectively. (G–I) XRD results of CRG@PVA with distinct M_w from 100K (a), 50K (b) to 16K (c), and 2K (d).

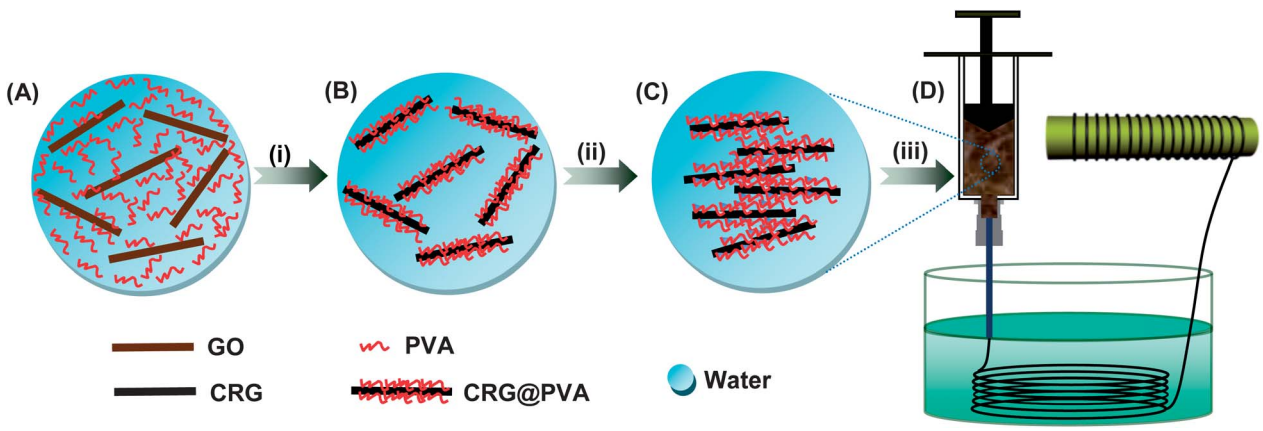

Scheme 1 Preparation of CRG@PVA spinning dope and cartoon of the spinning apparatus. (A) aqueous solution containing GO and PVA. (B) CRG@PVA solution after removing the free PVA. (C) Pre-aligned liquid crystalline CRG@PVA. (D) Wet-spinning assembly for preparation of continuous nacre-mimic fibers.

Comparing the cross profiles of CRG@PVA with different *R*, we find that the edges of CRG become fuzzy and neighboring sheets stick more tightly with increasing *R* (Fig. S7†). The layered structures were also observed for thicker fibers (Fig. S6†) and fibers with different M_w of PVA (2K, 16K, 50K and 100K) (Fig. S8†).

The as-prepared fibers are flexible and rigid. They can be tied into a compact knot even under dry conditions (see Fig. 4G and video 1 in ESI†), and can act like a spring, returning back to its original length after the external force removed (see video 2 in ESI†). Due to the homogeneous dispersibility of CRG@PVA in the spinning dope, the fibers can be spun uniformly and continuously for kilometers (Fig. 4H). As long as the feed stock permits, the fibers can be made longer.

The typical stress–strain curve of the nacre-mimicking CRG@PVA fibers is shown in Fig. 5A. CRG@PVA fibers exhibit an elastic behavior before the strain reaches 0.5% and a plastic

 This journal is © The Royal Society of Chemistry 2013

Published on 12 March 2013. Downloaded by Zhejiang University on 26/02/2014 07:47:31.

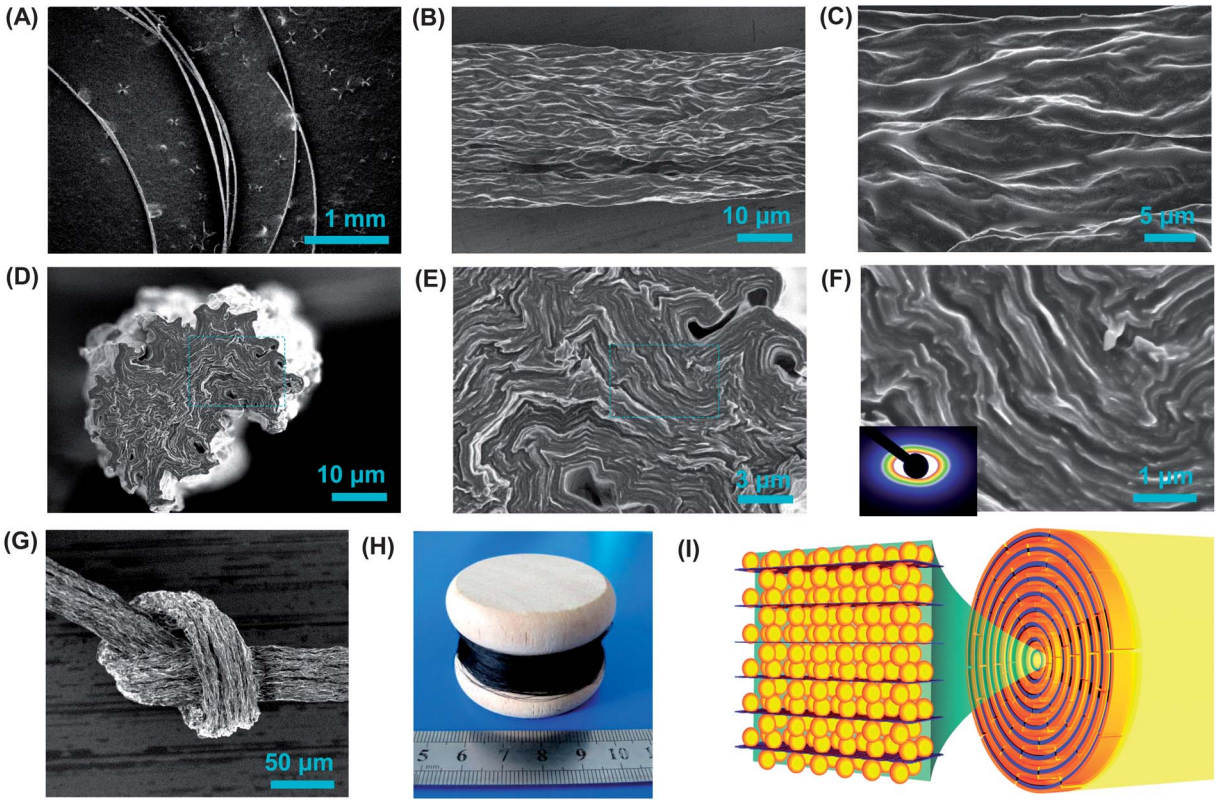

Fig. 4 Micro- and macro-structures of CRG@PVA fibers. (A–C) SEM images of a fiber with different magnifications. (D–F) The cross-section images of the fiber, the inset of (F) is the SAXS 2D pattern of the fiber. (G) A knot of CRG@PVA fiber, demonstrating the good flexibility of the fiber. (H) Digital photograph of a kilometer-long fiber. (I) Cartoon diagram of the nanostructured layered fiber, the yellow particles represent PVA molecules, which coated on CRG tightly and played a role of mortar sticking the CRG together.

behavior when the strain is between 0.5 and 2.9%, in an identical manner to the shear-lag model for nacre.[37] As the strain approaches 0.5%, the interface of PVA layers start to yield in shear and the CRG@PVA building blocks slide away from each other, along with the destruction and reconstruction of the hydrogen bonding network between PVA chains and CRG. The tensile load is then transferred from the soft PVA molecules to the hard graphene sheets with increasing strain. Then the shear spreads all over the fiber and finally the fibers are fractured by the pulling out of CRG@PVA building blocks (Fig. 5H). The fracture mechanism is proved by SEM observation of the fracture surfaces. As shown in Fig. 5D–G, the CRG@PVA building blocks are pulled out from the fiber, leading to interspaces between building blocks.

Compared with the pure PVA fiber (Fig. 5B, curve a), the tensile strength (σ) of CRG@PVA fiber is increased by 95% from 86 to 161 MPa. Even though the composite was incorporated with 63.5 wt% of soft polymer, its σ is greater than those of neat GO fiber (102 MPa) and CRG fiber (140 MPa).[36] Hence, the nacre-mimicking fiber is stronger than both of the neat PVA and CRG components. The σ of CRG@PVA fiber is also higher than those of nacre (~140 MPa)[38] and some nacre-mimicking materials such as montmorillonite-polyimide (MTM-PI) (70–80 MPa),[5] montmorillonite-chitosan (MTM-C) (100 MPa),[6] layered double hydroxides-chitosan (LDH-C) (160 MPa),[9] GO-PVA (110 MPa),[17] HPG-TRG (125 MPa),[22] and montmorillonite-poly(diallyldimethylammonium) chloride (MTM-PDMA) (109 MPa),[39] (Fig. 5C). The Young's modulus (E) is increased by 362% from 2.1 GPa for pure PVA fiber to 9.9 GPa for CRG@PVA fiber (Fig. 5B, curve b). The σ and E are further increased to *ca.* 200 MPa and 17.1 GPa by immersing the CRG@PVA fiber in 5 wt% PVA solution for one day to fill and repair the fiber voids (Fig. 5B, curve c). The PVA-soaked CRG@PVA fiber is very strong and stiff, and its σ and E are both higher than other nacre-mimicking materials including graphene-based composites.[37,40,41] Theoretical calculations and simulations show that high σ (1.7 GPa) and E (34 GPa) are accessible due to the large amount of hydrogen bonding between GO and PVA,[42] so there is much space for mechanical improvement of our CRG@PVA fibers by optimization of assembly conditions.

The as-prepared fibers are quite stable in water even after soaking for a month. The σ is almost retained (141 MPa), while the toughness is largely improved and the break elongation can reach 11% (Fig. 5B, curve d). The σ of CRG@PVA fiber is higher than that of GO@PVA fiber without reduction (130 MPa) (Fig. 5B, curve e), likely due to the restoration of a conjugated π–π network after chemical reduction. Interestingly, the σ of fibers increased from 81 to 161 MPa as the f_{PVA} was improved from 53.1 to 65.8% (Table 1), because of the better dispersibility of CRG with higher PVA content. For the identical f_{PVA} of 65.8%, the σ of fiber (161 MPa) is higher than the corresponding film (107 MPa) (Fig. S10†).

Published on 12 March 2013. Downloaded by Zhejiang University on 26/02/2014 07:47:31.

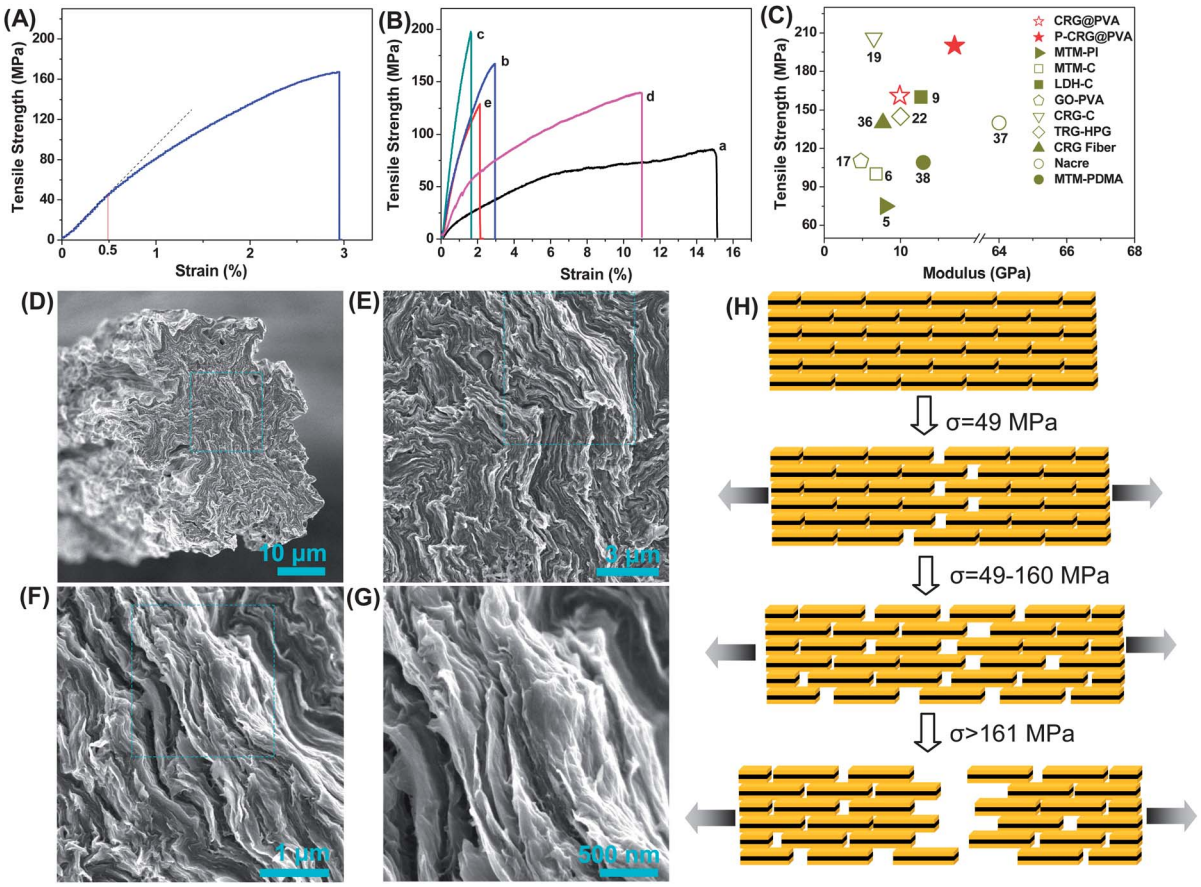

Fig. 5 (A) Typical stress–strain curve of CRG@PVA fiber; (B) typical stress–strain curves of neat PVA fiber (a), CRG@PVA fiber (b), CRG@PVA fiber soaked in PVA aqueous solution for 24 hours (c), CRG@PVA fiber immersed in water for a month (d), and GO@PVA fiber (e). (C) Comparison of σ and E with a set of nacre-mimicking nanocomposites. (D–G) Fracture surface images of the CRG@PVA fiber at different magnifications. (H) Schematic diagram illustrating the whole of the fracture process of nacre-mimicking CRG@PVA fibers.

The good mechanical performance of the CRG@PVA fibers is mainly attributed to the strong interaction between PVA and CRG. Based on the pull-out mode for the fracture, σ mostly depends on the interface interaction of the adjacent building blocks. The fiber suffered mainly three kinds of force under tensile loading. Hydrogen bond interaction between adjacent building blocks is the first kind of force. Theoretical calculations of the PVA-GO nanocomposite paper show that hydrogen bond density is as high as 10 bonds per nm,[2,42] which is crucial to the good performance of the fibers. The friction between different PVA nanoclusters, proved by AFM images (Fig. 1), is also responsible for the final σ. Microscale wrinkles of building blocks (Fig. 4) lead to additional friction, explaining the phenomenon of the higher strength for fibers than that for films. So our fibers, combining aligned hydrogen bonding with hierarchical structures, outperform most of other artificial layered nanocomposites in mechanical strength.

To further investigate the M_w effect of PVA on the mechanical performance of CRG@PVA fibers, we prepared CRG@PVA fibers with M_w of 2K, 16K, 50K and 100K, respectively. R is 20 for all samples. The testing results showed that the σ values for CRG@PVA fibers composed of different M_w of PVA were all around 160 MPa (Table 1), indicating that M_w of polymer layer has no effect on the mechanical properties of such nacre-mimicking composites. This breaks the rule of common polymer materials whose mechanical strength is improved with increasing M_w. We probed the preliminary reason behind this peculiar phenomenon by DSC measurements. As shown in Fig. 6A–D, pure PVA samples show obvious melting and crystallization peaks as well as glass transition temperature (T_g) (see the amplified images in Fig. 6E–H), whereas no peak or T_g is observed for any of the CRG@PVA composite samples during the test temperature. It is well known that T_g is related to the motion of polymer chains. Qualitatively, the motion of the polymer chains in glass transition region can be interpreted as long-range, coordinated molecular motion. For pure PVA, the chains complete this motion in the glass transition region. Polymers with higher M_w need higher thermal energy to carry out the long-range, coordinated molecular motion, leading to higher T_g. So T_gs of pure PVA are increased from 63.6 °C for PVA 2K, to 71.7 °C for PVA 16K, 71.8 °C for PVA 50K and to 73.1 °C for PVA 100K. However, for CRG@PVA building blocks, PVA chains are constrained in a tiny and fixed space between two adjacent CRG sheets by strong hydrogen bonding. In such a circumstance, the motion of PVA chains is completely confined, resulting in the disappearance of T_g for PVA chains of

 This journal is © The Royal Society of Chemistry 2013

Published on 12 March 2013. Downloaded by Zhejiang University on 26/02/2014 07:47:31.

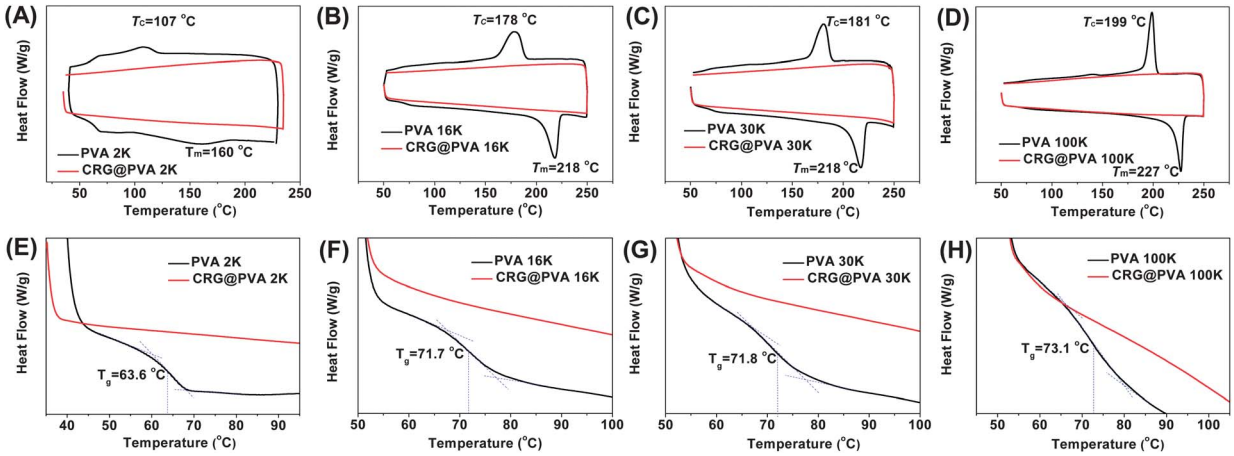

Fig. 6 DSC curves of pure PVA and CRG@PVA with PVA M_w of 2K (A), 16K (B), 50K (C) and 100K (D). T_g regions of pure PVA and CRG@PVA with M_w of 2K (E), 16K (F), 50K (G) and 100K (H).

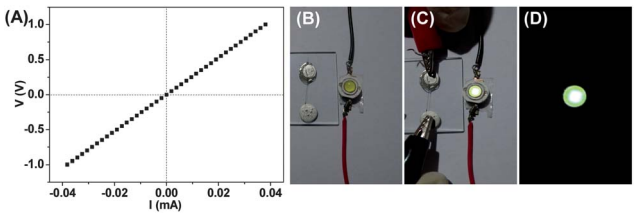

Fig. 7 (A) *I–V* curve of the CRG@PVA fiber with *R* of 1.75. LED circuit without (B) and with (C) connection of CRG@PVA fiber. (D) The emission of the LED lamp in the dark.

CRG@PVA. Besides T_g, melting and crystallization peaks also vanished for CRG@PVA samples for the same reason. Therefore, M_w of PVA has no influence on the mechanical properties of CRG@PVA composites. This indicates that the operating temperature of polymers can be highly improved by the formation of nacre-mimicking structures, which is extremely important for engineering materials used in high-temperature environments.

Superior to other layered materials, graphene-based nacre mimics should be electrically conductive due to the conductive nature of CRG. The electrical conductivity is decreased with increasing f_{PVA} for both CRG@PVA papers and fibers (Fig. S11†). Due to the different saturated adsorption capacity, the conductivity of composites decreased from 0.103 S m^{-1} for CRG@PVA 2K to 0.036 S m^{-1} for CRG@PVA 16K, 0.022 S m^{-1} for CRG@PVA 50K and to 0.013 S m^{-1} for CRG@PVA 100K (see Fig. S11†). Using hydroiodic acid treatment,[43] the conductivity of CRG@PVA with *R* of 1.75 fiber is improved by 437 times from 0.8 to 350 S m^{-1}. The as-prepared single fiber even can be used as a wire to light an LED lamp (Fig. 7).

Conclusions

In conclusion, we fabricated for the first time continuous high-content CRG-based composite fibers with lengths of kilometers by an industrially viable wet-spinning assembly strategy. The fibers are characterized by the fine B&M structures, where CRG serves as hard bricks and PVA as sticky mortar. The fibers are strong, exceeding nacre and most of the artificial layered materials. The mechanical strength and electrical conductivity of the nacre-mimicking fibers are related to the coated PVA content. Distinguished from typical polymers and composites, M_w of PVA has no effect on the mechanical performance of the fibers because the motion of PVA chains are confined in the nanochannels between the adjacent CRG sheets. The nacre-mimicking fibers are also electrically conductive, a unique property that other layered materials do not possess, and the single fiber can be even used as a wire to light an LED lamp. The combination of facile large-scale availability, excellent mechanical properties, good electrical conductivity, and molecular weight-independent strength for the nacre-mimicking fibers promises wide applications in engineering materials, functional fibers, antistatic textiles, and wearable supercapacitors.

Acknowledgements

This work is funded by the National Natural Science Foundation of China (no. 20974093 and no. 51173162), Qianjiang Talent Foundation of Zhejiang Province (no. 2010R10021), Fundamental Research Funds for the Central Universities (no. 2013XZZX003), Research Fund for the Doctoral Program of Higher Education of China (no. 20100101110049) and Zhejiang Provincial Natural Science Foundation of China (no. R4110175).

Notes and references

1 M. Moniruzzaman and K. I. Winey, *Macromolecules*, 2006, **39**, 5194–5205.
2 H. B. Yao, H. Y. Fang, Z. H. Tan, L. H. Wu and S. H. Yu, *Angew. Chem., Int. Ed.*, 2010, **49**, 2140–2145.
3 P. Podsiadlo, A. K. Kaushik, E. M. Arruda, A. M. Waas, B. S. Shim, J. Xu, H. Nandivada, B. G. Pumplin, J. Lahann, A. Ramamoorthy and N. A. Kotov, *Science*, 2007, **318**, 80–83.

Published on 12 March 2013. Downloaded by Zhejiang University on 26/02/2014 07:47:31.

4 B. Long, C. A. Wang, W. Lin, Y. Huang and J. L. Sun, *Compos. Sci. Technol.*, 2007, **67**, 2770–2774.
5 R. Chen, C. A. Wang, Y. Huang and H. Le, *Mater. Sci. Eng., C*, 2008, **28**, 218–222.
6 H. B. Yao, Z. H. Tan, H. Y. Fang and S. H. Yu, *Angew. Chem., Int. Ed.*, 2010, **49**, 10127–10131.
7 L. J. Bonderer, A. R. Studart and L. J. Gauckler, *Science*, 2008, **319**, 1069–1073.
8 E. Munch, M. E. Launey, D. H. Alsem, E. Saiz, A. P. Tomsia and R. O. Ritchie, *Science*, 2008, **322**, 1516–1520.
9 J. B. Han, Y. B. Dou, M. Wei, D. G. Evans and X. Duan, *Angew. Chem., Int. Ed.*, 2010, **49**, 2171–2174.
10 T. Kato, *Adv. Mater.*, 2000, **12**, 1543–1546.
11 K. W. Putz, O. C. Compton, M. J. Palmeri, S. T. Nguyen and L. C. Brinson, *Adv. Funct. Mater.*, 2010, **20**, 3322–3329.
12 A. Tao, P. Sinsermsuksakul and P. Yang, *Nat. Nanotechnol.*, 2007, **2**, 435–440.
13 S. Deville, E. Saiz, R. K. Nalla and A. P. Tomsia, *Science*, 2006, **311**, 515–518.
14 S. Park and R. S. Ruoff, *Nat. Nanotechnol.*, 2009, **4**, 217–224.
15 J. Liang, Y. Huang, L. Zhang, Y. Wang, Y. Ma, T. Guo and Y. Chen, *Adv. Funct. Mater.*, 2009, **19**, 2297–2302.
16 C. Bao, Y. Guo, L. Song and Y. Hu, *J. Mater. Chem.*, 2011, **21**, 13942–13950.
17 Y. Xu, W. Hong, H. Bai, C. Li and G. Q. Shi, *Carbon*, 2009, **47**, 3538–3543.
18 Y. Li, T. Yang, T. Yu, L. Zheng and K. Liao, *J. Mater. Chem.*, 2011, **21**, 10844–10851.
19 X. Wang, H. Bai, Z. Yao, A. Liu and G. Q. Shi, *J. Mater. Chem.*, 2010, **20**, 9032–9036.
20 X. Zhao, Q. Zhang, D. Chen and P. Lu, *Macromolecules*, 2010, **43**, 2357–2363.
21 Y. Q. Li, T. Yu, T. Y. Yang, L. X. Zheng and K. Liao, *Adv. Mater.*, 2012, **24**, 3426–3431.
22 X. Z. Hu, Z. Xu and C. Gao, *Sci. Rep.*, 2012, **2**, 767.
23 L. Kou, H. K. He and C. Gao, *Nano-Micro Lett.*, 2010, **2**, 177–183.
24 L. Kou and C. Gao, *Nanoscale*, 2011, **3**, 519–528.
25 H. K. He and C. Gao, *Chem. Mater.*, 2010, **22**, 5054–5064.
26 V. C. Tung, M. J. Allen, Y. Yang and R. B. Kaner, *Nat. Nanotechnol.*, 2009, **4**, 25–29.
27 X. Yang, L. Li, S. Shang and X. M. Tao, *Polymer*, 2010, **51**, 3431–3435.
28 D. Li, M. B. Müller, S. Gilje, R. B. Kaner and G. G. Wallace, *Nat. Nanotechnol.*, 2008, **3**, 101–105.
29 H. Kong, C. Gao and D. Y. Yan, *Macromolecules*, 2004, **37**, 4022–4030.
30 T. N. Blanton and D. Majumdar, *Powder Diffr.*, 2012, **27**, 104–107.
31 X. Huang, Z. Y. Yin, S. X. Wu, X. Y. Qi, Q. Y. He, Q. C. Zhang, Q. Y. Yan, F. Boey and H. Zhang, *Small*, 2011, **7**, 1876–1902.
32 X. Huang, X. Y. Qi, F. Boey and H. Zhang, *Chem. Soc. Rev.*, 2012, **41**, 666–686.
33 Z. Xu, H. Y. Sun, X. L. Zhao and C. Gao, *Adv. Mater.*, 2013, **25**, 188–193.
34 Z. L. Dong, C. C. Jiang, H. H. Cheng, Y. Zhao, G. Q. Shi, L. Jiang and L. T. Qu, *Adv. Mater.*, 2012, **24**, 1856–1861.
35 C. G. Hu, Y. Zhao, H. H. Cheng, Y. H. Wang, Z. L. Dong, C. C. Jiang, X. Q. Zhai, L. Jiang and L. T. Qu, *Nano Lett.*, 2012, **12**, 5879–5884.
36 Z. Xu and C. Gao, *Nat. Commun.*, 2011, **2**, 571.
37 J. F. Wang, Q. F. Cheng and Z. Y. Tang, *Chem. Soc. Rev.*, 2012, **41**, 1111–1129.
38 A. P. Jackson, J. F. V. Vincent and R. M. Turner, *Proc. R. Soc. London, Ser. B*, 1988, **234**, 415–440.
39 Z. Tang, N. A. Kotov, S. Magonov and B. Ozturk, *Nat. Mater.*, 2003, **2**, 413–418.
40 H. Chen, M. B. Müller, K. J. Gilmore, G. G. Wallace and D. Li, *Adv. Mater.*, 2008, **20**, 3557–3561.
41 Z. An, O. C. Compton, K. W. Putz, L. C. Brinson and S. T. Nguyen, *Adv. Mater.*, 2011, **23**, 3842–3846.
42 O. C. Compton, S. W. Cranford, K. W. Putz, A. Zhi, L. C. Brinson, M. J. Buehler and S. T. Nguyen, *ACS Nano*, 2012, **6**, 2008–2019.
43 S. F. Pei, J. P. Zhao, J. H. Du, W. C. Ren and H. M. Cheng, *Carbon*, 2010, **48**, 4466–4474.

 This journal is © The Royal Society of Chemistry 2013